Energy Conversion and Management 74 (2013) 51–59

Contents lists available at SciVerse ScienceDirect

Energy Conversion and Management

journal homepage: www.elsevier.com/locate/enconman

Optimal electrical load for peak power of a thermoelectric module with a solar electric application

Frédéric J. Lesage [a,b,*], Rémi Pelletier [a], Luc Fournier [a], Éric V. Sempels [c]

[a] Cégep de l'Outaouais, 333 boul. de la Cité-des-Jeunes, Gatineau, Canada J8Y 6M4
[b] McMaster University, 1280 Main Street West, Hamilton, Canada L8S 4L7
[c] École Polytechnique de Montréal, 2900 Boulevard Edouard-Montpetit, Montréal, Canada QC H3T

ARTICLE INFO

Article history:
Received 23 February 2013
Accepted 5 May 2013
Available online 31 May 2013

Keywords:
Thermopower
Thermoelectric module
Electrical load
Load matching
Solar thermoelectric conversion

ABSTRACT

This paper builds upon the recent progress made in the field of thermoelectric energy conversion when using Bismuth Telluride Bi_2Te_3 semiconductor modules. These commercially available modules have been the subject of many recent studies in which the common goal is to better understand their thermoelectric behavior when converting a low cost heat source to electricity. The present experimental work investigates the thermopower properties of a single module relative to the electrical load resistance with the use of two experimental apparatuses. The first test stand is built with a precision control of the injection and rejection of heat to and from the module; the second test stand is a novel demonstration of the module's application to thermoelectric solar energy conversion. The thermopower characteristics of the module are measured over a wide range of thermal input conditions. The results highlight the importance in calibrating to an optimal electrical load for peak power output. A normalized thermopower theoretical evolution curve relative to load resistance is presented. Furthermore, a method of thermoelectric recovery of solar radiation is demonstrated using laboratory controlled working conditions.

© 2013 Elsevier Ltd. All rights reserved.

1. Introduction

In order to investigate new methods of harnessing solar energy, thermoelectric modules are now being considered for its ability to convert solar radiation to electricity amongst other low cost heat sources [1–3]. Indeed, Refs. [4–7] outline the thermoelectric potential of vehicle exhaust, Ref. [8] describes a liquid-to-liquid thermoelectric generator for waste-heat recovery applications, Ref. [9] demonstrates a successful biomass cook stove application and Ref. [10] details the potential of a thermoelectric conversion of solar radiation. The thermoelectric recovery of solar energy has been tested by Ref. [11] in which heat resulting from solar radiation is conducted to a thermoelectric module through an aluminum bloc. In their study, it was shown that it is necessary to improve the concentration of solar radiation when applying it to the thermoelectric effect. To this end, Refs. [12,13] used Fresnel lens' to focalise an ensemble of solar rays onto the surface of a module. The shortcoming of their system was that the concentration of solar radiation was not evenly distributed over the surface of the module. In an effort to use the excess heat from photovoltaic solar panels, Refs. [14,15] placed thermoelectric modules adjacent to the panels. The coupling of these technologies is currently limited by the temperature gradient necessary for effective thermoelectric conversion. More recently, Ref. [16] combined thermoelectric technology with that of solar vacuumed tubes. In their study, the energy captured is driven to a single module via a heat pipe. Despite improving the available temperature gradient across the module, the relative geometries of the heat pipe and the thermoelectric module limit the available contact surface.

For these applications and many others, the semi-conductors Bismuth Telluride (Bi_2Te_3) were shown by Refs. [17–19] to be the most efficient materials for exploiting the thermoelectric phenomenon within the temperature range of 273–473 K. For this reason, many works focus on better understanding the thermoelectric characteristics of Bi_2Te_3 Refs. [20–23]. More recently, optimization methods for systems using thermoelectric modules inserted into a liquid-to-liquid generator were presented by Ref. [24] who showed that power output can be almost doubled with favorable inner turbulence and by Ref. [25] who showed that the thermoelectric peak power is very sensitive to the electrical load resistance and that the optimal load resistance is less than the internal resistance of the system. The importance in properly identifying the electrical load is detailed in discussions on Maximum Power Point Tracking (MPPT) in the thermoelectric works of Refs. [26–28].

The current experimental study builds upon the results of Ref. [25] by investigating the optimal electrical load resistance and its

* Corresponding author at: Cégep de l'Outaouais, 333 boul. de la Cité -des-Jeunes, Gatineau, Canada J8Y 6M4. Tel.: +1 819 770 4012; fax: +1 819 770 8167.
E-mail addresses: Frederic.Lesage@cegepoutaouais.qc.ca (F.J. Lesage), Remi.Pelletier@cegepoutaouais.qc.ca (R. Pelletier), Luc.Fournier@cegepoutaouais.qc.ca (L. Fournier), eric_sempels@hotmail.com (É.V. Sempels).

0196-8904/$ - see front matter © 2013 Elsevier Ltd. All rights reserved.
http://dx.doi.org/10.1016/j.enconman.2013.05.008

Nomenclature

A	contact area of a thermocouple pellet (m^2)	P	power (W)
H	hot side	P^*	P/P_{max}
C	cold Side	$\dot{q}$	thermal energy generation per unit volume (W/m^3)
i	internal	R	electrical resistance (Ω)
I	electrical current (A)	R^*	R/R_i (Ω)
L	load	T	temperature (K)
k	thermal conductivity W/m K	V	voltage (A)
max	maximum	V^+	V/V_{oc},
oc	open circuit	$\alpha_{p,n}$	Seebeck coefficient (V/K)
opt	optimal	ρ	electrical resistivity (Ω m)

related characteristics for a single thermoelectric module. In particular, the thermopower characteristics for varying temperature fields relative to an increasing electrical load are reported and discussed. To this end, a noncomplicated test apparatus is built in which a controlled heat input is applied to one side of a Bi_2Te_3 thermoelectric module and a controlled heat diffusion is maintained on its opposite side resulting is a stable thermal field across the module. Furthermore, a novel thermoelectric application to solar radiation is built and tested. Both test apparatuses are equipped with a rheostat which increases the electrical load yielding precision measurements of the optimal load relative to the internal electrical resistance. It is shown that: a varying temperature field has negligible effects on the ratio of the electrical load to internal resistance of the module; at peak power, the electrical load is strictly less than the internal resistance; identifying the optimal electrical load is necessary for peak thermopower.

2. Thermopower and electric load matching

The underlying physics of the present study pertain to the power output of a thermoelectric element relative to its electrical load resistance R_L. In particular, a better understanding of the relation between R_L and the internal electrical resistance (noted R_i) is sought. For the purpose of the discussions that follow, a detailed account of the electromotive force generated by a semiconductor subject to a thermal field e.g. Refs. [29,30] is provided with a particular attention to the commonly used load matching result.

In order to generate the thermopower production known as the Seebeck effect, crystalline structured semiconductors are doped such that n type semiconductors favor negative charge carrier mobility and p type semiconductors favor positive charge carrier mobility. This is best accomplished by combining two chemical elements for which the difference in the number of their respective valence electrons is one. In this way, through a natural mutual attraction, the resultant crystalline lattice either has a single "free" valence electron in the outer shells of its atoms or a "hole" in the outer shells of its atoms depending on how they are doped. The "free" single valence electrons easily migrate to neighboring atoms and are referred to as negative charge carriers. Conversely, the "holes" attract electrons from neighboring atoms thereby transferring the location of the "hole" and are referred to as positive charge carriers. For example, in this study, the chemical elements Bismuth and Tellurium, having five and six valence electrons respectively, are combined into the crystalline structure Bi_2Te_3. The resultant material, when subject to a difference in temperature at its extremities, produces an electromotive force which mobilizes charge carriers from a hot pole to a cold pole. As illustrated in Fig. 1, by coupling a negatively doped material with a positively doped material, an electric circuit can be created in which the charge carrier flow direction is unilateral.

The conservation of energy of the closed system and Fourier's law of conduction requires that the one dimensional form of the heat equation for the thermalcouple illustrated in Fig. 1, be of the form

$$\frac{d}{dx}\left(k\frac{dT}{dx}\right) - \dot{q} = 0 \tag{1}$$

in which $\dot{q}$ is the thermal energy generation per unit volume.

In assuming isotropic properties and equalized contact surfaces on the cold and hot side, Ohm's Law reduces the one dimensional heat equation to,

$$\frac{d^2T}{dx^2} + \frac{I^2\rho}{kA^2} = 0 \tag{2}$$

in which ρ and k are the electrical resistivity and the thermal conductivity respectively of the material, I is the electrical current and A is the contact surface. It is important to note that the sign change in the second term of Eq. (2) is due to the fact that the system's conversion of thermal to electrical reduces its total thermal energy. Furthermore, the calculation of the thermoelectric power of this study, the Thomson effect (which relates the passage of current in an electrical conductor subject to a thermal dipole to the reversible heat) is considered to be negligible. This effect is commonly neglected in low temperature thermoelectric applications Ref. [30]. Indeed, the Kelvin relationship states that the Thomson coefficient is proportional to the rate of change of the material's Seebeck coefficient with respect to temperature. As previously stated, the material properties in the present work are considered isotropic. Furthermore, the linear profile of the forthcoming electric tension

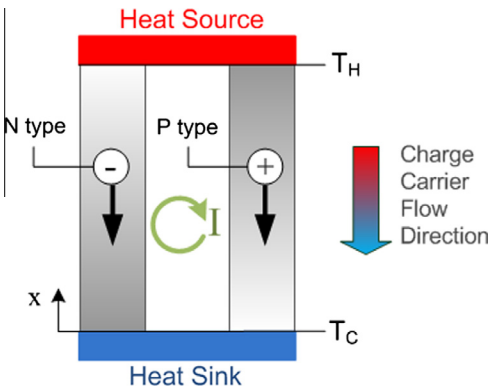

Fig. 1. Charge carrier flow direction for a thermocouple with n type and p type pellets in parallel.

results presented in Fig. 7 with respect to thermal variance suggest that the Seebeck coefficient for this study is invariant relative to temperature and as such the Thomson effect is considered negligible.

The temperature profile resulting from the boundary conditions T_H and T_C is used to develop the power output for a single thermocouple by considering the heat flux "in" to be equal to the heat flux "out" plus the heat converted to electricity. A detailed account of the thermopower output of a single thermocouple developed from the resultant temperature profile is given in Ref. [25] yielding,

$$P = \Delta T^2 \alpha_{p,n}^2 \frac{R_L}{(R_i + R_L)^2} \tag{3}$$

in which $\Delta T = T_H - T_C$ and $\alpha_{p,n}$ is the difference in the p type and n type Seebeck coefficients. The Seebeck coefficient of a material is an intrinsic part of its electronic structure and its thermopower capabilities.

Recalling that the current study focuses on the effects of an increasing load on the power production of a thermoelectric module, evaluating the thermopower's instantaneous rate of change with respect to the electrical load reveals a critical value at $R_L = R_i$. It is easily shown that this critical value yields a maximum thermopower. This result is referred to as electric load matching and is commonly used for thermoelectric peak power production e.g. Refs. [26,31,32]. From Eq. (3), assuming load matching, noted here as $R_{L=i}$, the peak power is simply,

$$P_{\max} = \frac{\Delta T^2 \alpha_{p,n}^2}{4R_{L=i}}. \tag{4}$$

It is important to note that the value ΔT in Eq. (3) is idealized as being the difference in the temperatures measured at the extremities of a unique pair of thermoelements and that the interconnecting materials are not considered in the calculation. Nevertheless, as demonstrated by Ref. [29], for N thermoelement pairs connected in series in the form of a module, the predicted optimal electrical load remains equal to the internal resistance.

The normalized thermopower evolution relative to load resistance can be expressed by considering the peak power expression of Eq. (4) as the characteristic term. Therefore, by combining Eq. (3) with Eq. (4), the normalized thermopower $P^* = P/P_{\max}$ becomes,

$$P^* = \frac{4R_L R_{L=i}}{(R_i + R_L)^2}. \tag{5}$$

In order to generate a single expression describing the thermopower evolution relative to the electrical resistance near the optimal load, Eq. (5) is further simplified by normalizing each resistance term by the internal resistance near peak power and simplifying the expression by generalizing the internal resistance as a constant value near the maximum point. The normalized thermopower $P^* = P/P_{\max}$ near peak power is therefore,

$$P^* = \frac{4R_L^*}{(1 + R_L^*)^2} \tag{6}$$

in which the normalized electrical load is defined as $R_L^* = R_L/R_i$.

The usefulness in the normalized power output curve in the management of energy systems is that it makes it possible to identify the optimal electrical load for peak power output under varying working conditions e.g. Ref. [25]. The importance in the result expressed in Eq. (6) is that P^* attains unity at peak power when R_L^* is also at unity and that this is true for all thermal input conditions. This is easily demonstrated by evaluating its rate of change relative to the normalized load,

$$\frac{dP^*}{dR_L^*} = \frac{4(1 - R_L^*)}{(1 + R_L^*)^3}. \tag{7}$$

In practical thermoelectric applications, in order to calibrate for peak thermopower, the electrical load voltage is measured and compared to the open circuit voltage. This is done with the use of circuit theory from which e.g. Refs. [31,33],

$$V_L^+ = \frac{R_L^*}{1 + R_L^*} \tag{8}$$

in which the load voltage is normalized by the open circuit voltage such that $V_L^+ = V_L/V_{oc}$. Since Eq. (6) states that peak power output occurs when R_L^* attains unity, the electrical load resistance of thermoelectrical systems are commonly calibrated to,

$$V_{L,opt}^+ = \frac{1}{2}. \tag{9}$$

The goal of the present study is to test the validity of Eqs. (6) and (9) when applied to a thermoelectric module under an increasing electrical load resistance. To this end, an experimental apparatus is built with precision testing of the thermopower output of a single module. The system is tested under a wide range of thermal input conditions with an increasing electrical load. Furthermore, peak thermopower is applied to a novel solar electric application.

3. Experimental setup

An experimental test stand is built in order to measure the thermopower of commercially available thermoelectric Bi_2Te_3 modules under an increasing electrical load. The test stand applies heat on one side of a thermoelectric module and dissipates heat on the other. As previously discussed, the resulting contrast in the temperature field generates an electromotive force driving an electric current. The TEG2-07025HT-SS thermoelectric module used is the present study is made up of alternating n type and p type Bi_2Te_3 semiconductor pellets connected electrically in series and held together by two ceramic layers. The module measures 40 mm × 40 mm × 3.75 mm.

The cold side of the module is subject to forced air convection by way of an ORIX MD625B-24-Q6 ventilation unit of dimensions 62 mm × 62 mm × 25.4 mm at a constant frequency of 200/3 Hz and a volumetric flow rate of 500 L/min. The hot side temperature is maintained by applying four heating wirewound resistors directly to the module. The resistors' heat input is controlled by a variable power supply LabVolt – 4194 with a DC output voltage that is measured using a Metex M-3800 multimeter to an accuracy of ±0.5%. In this way, it was made possible to adjust the temperature of each heating resistor. Pressure is applied to the resistors by way of a 2.2 kg weight with a uniform mass distribution and a contact area with the resistors of 12.42 cm^2. A thermal compound Omegatherm 201 is placed between the resistors and the thermoelectric modules in order to improve the thermal exchange between them. The temperature difference across the module is measured by way of four Omega SA1-T-72 sensors evenly spaced and flush to the surface on each side of the module. The resultant temperature difference is measured to be within an uncertainty of ±0.5 °C.

A rheostat effectively varies the load resistance imposed on the system by decompressing stacked horizontal carbon plates which are in contact with one another. Decompressing the plates degenerates the electrical connexion between them causing the load resistance applied to the system to increase from 0 to 100 Ω. Data acquisitioning is performed with DataStudio software in which the sensors of the test stand are able to communicate with the computer via the interface ScienceWorkshop 750. The resultant voltage readings are of an accuracy of ±3 mV. A schematic representation of the experimental apparatus is provided in Fig. 2.

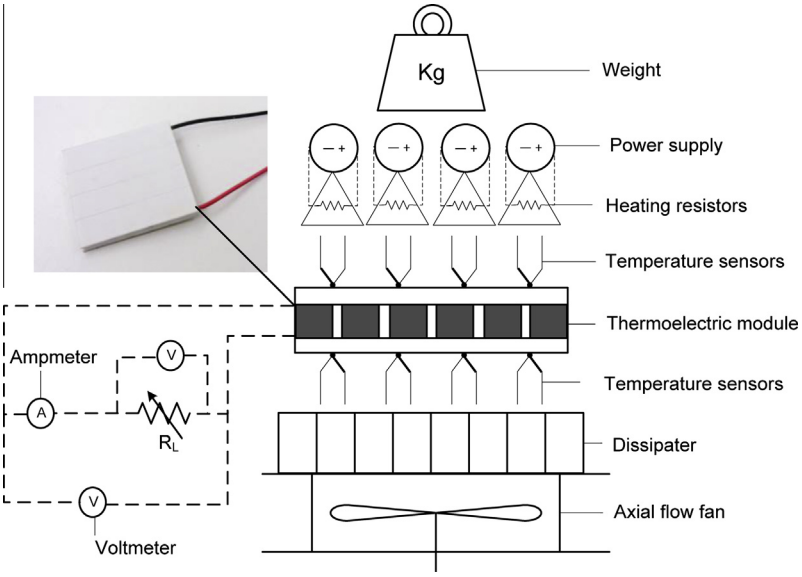

Fig. 2. Schematic representation of the injection and rejection of heat to the thermoelectric module.

The ability to increase the electrical load resistance while measuring its value as well is its time rate of change is central to the success of this study. Care is taken to build an apparatus which allows for precision measurements and a varying load. To this end, a motor's rotational speed is translated into a linear digression of a carbon plate on one end of the rheostat thereby releasing pressure on the entire set of carbon plates and increasing the electric load resistivity. The electrical load for all test cases is increased at a rate of 1.8 ± 1.6 Ω/s. A variable power supply to the motor is controlled with a LabVolt – 4194 and a reverse switch is used to alternate the motor direction. The load resistance is calculated by measuring the voltage and current at the load resistance terminal. The schematic representation of the rheostat providing the variable load resistance is illustrated in Fig. 3. It is important to note that the variable load described in Fig. 3 is represented simply as a dynamic load resistance in Fig. 2.

4. Results and discussion

In an effort to identify the peak power performance of the module relative to the electrical load and to the temperature profile, the thermopower performance of a single module is measured for a large range of thermal input conditions. The temperature profiles are distinguished by the temperature difference, noted ΔT, between the hot side and the cold side of the module. The resultant ΔT's range from 14.5 to 104.0 °C and are detailed in Table 1.

4.1. Thermopower profiles relative to an increasing electrical load

The first set of results compiles the thermoelectric power output profiles relative to an increasing electrical load for the lower temperature range of thermal input conditions tested. The results are illustrated in Fig. 4 showing similar trends for all of the test cases. More specifically, as expected and predicted by Eq. (3), an increase in ΔT implies an increase in thermopower output. It is also observed that as the electrical load increases, the power output of the module increases sharply before attaining a maximum at an optimal electrical load after which it decreases at a more gradual slope.

The thermopower relative to an increasing electrical load is further tested for an upper temperature range, the results of which are presented in Fig. 5. Similar trends to that of the lower temperature input conditions are observed featuring a gradual decline in thermopower after attaining a maximum.

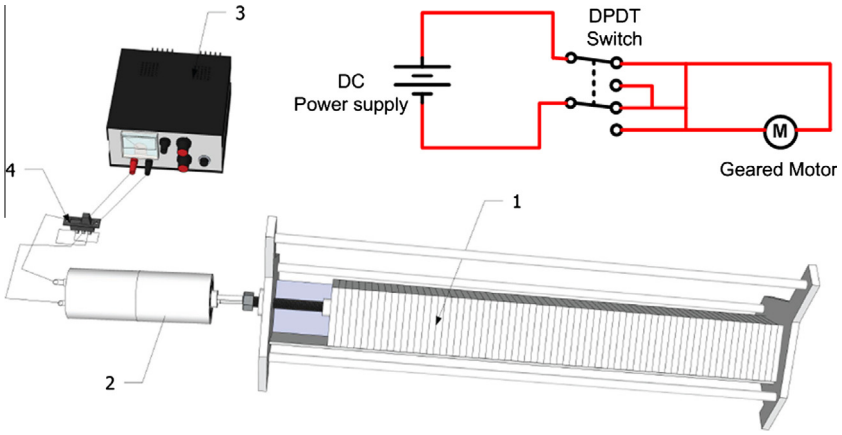

Fig. 3. Schematic representation of dynamic load resistance apparatus: (1) Carbon plate rheostat; (2) DC Geared motor; (3) DC Power supply; (4) Double pole, double terminal (DPDT) switch.

Table 1
Temperature readings on the hot side and cold side of the module.

ΔT (°C)	14.5	21.3	29.8	36.5	44.5	51.5	59.3	67.5	72.0	82.5	89.8	96.5	104.0
T_H (°C)	40.8	49.5	60.8	69.8	80.5	90.5	100.3	110.5	117.0	130.5	142.5	150.5	160.0
T_C (°C)	26.3	28.3	31.0	33.3	36.0	39.0	41.0	43.0	45.0	48.0	52.8	54.0	56.0

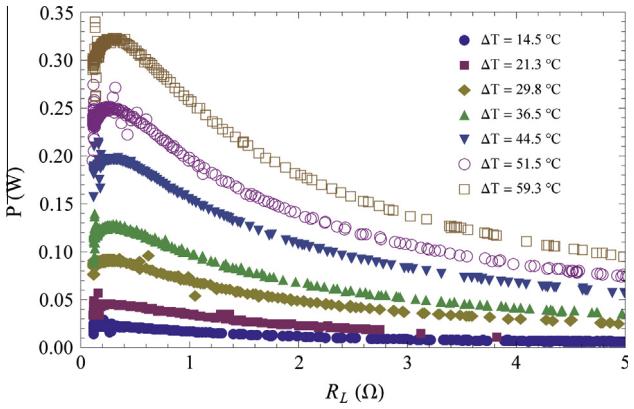

Fig. 4. Effect of an increasing electrical load resistance on thermopower output for thermal input conditions ranging from ΔT = 14.5–59.3 °C.

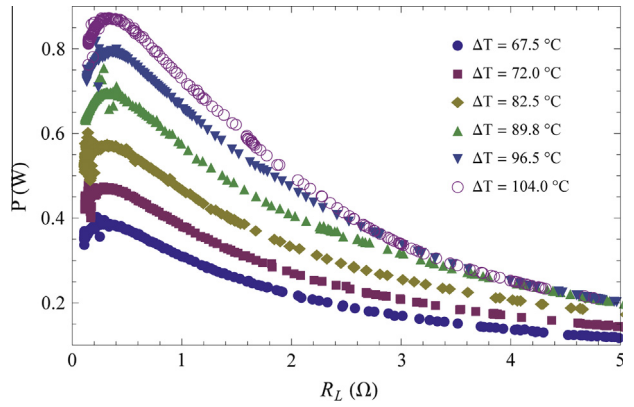

Fig. 5. Effect of an increasing electrical load resistance on thermopower output for thermal input conditions ranging from ΔT = 67.5–104.0 °C.

4.2. Peak thermopower characteristics

In an effort to examine peak power characteristics, the maximum coordinate points from Figs. 4 and 5 are plotted in Fig. 6 with respect to the temperature difference across the module. The power output and the load resistance at the maximum coordinate points for each temperature difference tested are noted $P_{\max}$ and $R_{L,opt}$ respectively. Furthermore, in order to examine the validity of the result, that peak power is obtained when load matching, the module's internal resistance and the normalized electrical load at maximum power, noted $R_{i,opt}$ and $R^*_{L,opt}$, are included in Fig. 6.

The results illustrated in Fig. 6 show a peak thermopower output curve that is proportional to the square of ΔT by a factor of 8.5×10^{-5}. This result corresponds well with Eq. (4) which predicts a parabolic peak thermopower curve with respect to ΔT. More notable are the electrical load and internal resistance curves. These curves show that the optimal electrical load and the internal resistance for peak power conditions each increase linearly with slopes of approximately 0.001 and 0.002 respectively. Since both the load and internal resistances are linear relative to the thermal input conditions, their ratio (namely $R^*_{L,opt}$) is necessarily constant with respect to ΔT. In particular, Fig. 6 shows the measured normalized optimal electrical load to be equal to the constant 0.5 relative to the thermal input conditions. The importance of this result lies in the fact that the measured peak power does not occur under load matching conditions but rather for an electrical load equal to half the internal electrical resistance. More precisely, the measured optimal electrical load is not that which is predicted by Eq. (3). Eq. (3) does however correctly predict it to be invariant with respect to changing thermal input conditions.

These results imply that, in application, the optimal conditions can be identified using one set of thermal input conditions and then applied to a wide range of thermal input conditions. In order to achieve such calibrations, it is necessary to identify $V^+_{L,opt}$. It is important to recall that this optimal normalized load voltage is derived from circuit theory under load matching to be 0.5. To examine its validity, the profiles relative to the thermal input conditions of the open circuit voltage and load voltage for the measured peak power performances, noted V_{oc} and $V_{L,opt}$, are presented in Fig. 7.

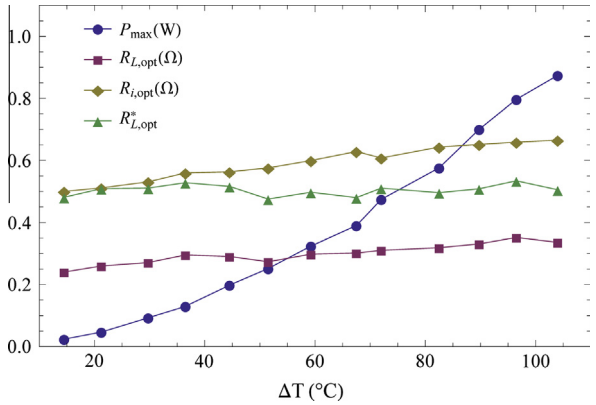

Fig. 6. Maximum power output and associated electrical resistance trends with respect to temperature difference across the module.

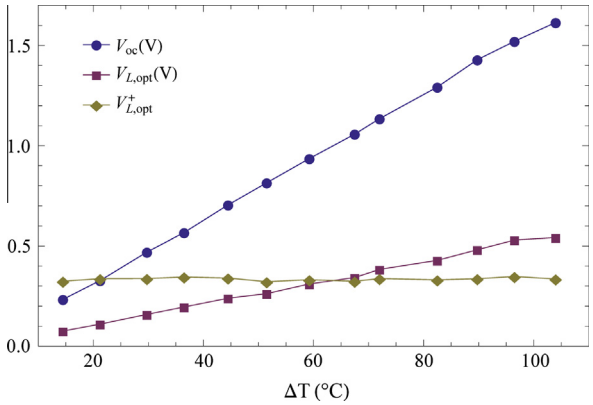

Fig. 7. Open circuit voltage and load voltage for measured peak power output trends with respect to temperature difference across the module.

In Fig. 7, the open circuit voltage and the load voltage are each shown to increase linearly relative to ΔT with slopes of 0.0157 and 0.00529 respectively. The linear profiles imply that the normalized optimal voltage, noted $V^{+}_{L,opt}$, is a constant. Indeed, it is measured from the results of Fig. 7 to be $V^{+}_{L,opt} = 0.335$. This result is noteworthy since it is less than the value predicted by Eq. (9) and since it confirms that the normalized optimal load voltage is invariant with respect to changing thermal input conditions.

4.3. Normalized thermopower curves

In an effort to evaluate optimal electrical load, the load evolution curves for the temperature fields presented in Fig. 4 are normalized by the peak thermopower obtained in each test case. In this way, peak power is attained at unity and the optimal electrical load can be identified from the resultant coordinate point. The results illustrated in Fig. 8 show that the power output evolution relative to the normalized electrical load for all ΔT collapse to a single normalized curve.

The normalized power output curves are further evaluated for the upper temperature thermal input conditions. Once again, it is observed that the normalized curves for all test cases collapse onto a common normalized profile. The results from the upper temperature profiles are presented in Fig. 9.

The trends observed in Figs. 8 and 9 show that the normalized thermopower output for all input conditions increase at the same rate relative to the normalized load to a maximum point beyond which there is a more gradual decrease in normalized thermopower. In the following section, these trends are further discussed in the context of a generalized normalized thermopower output curve.

4.4. Measured thermopower trends

In order to better evaluate the generalized trends of the thermopower output and to evaluate the validity of Eq. (6), the thermopower output curve relative to the electrical load generated by the ensemble of the measured values from all of the thermal input conditions is best fit to an 8th order polynomial curve. The results are illustrated in Fig. 10 along with the evolution of the normalized thermopower rate of change relative to the normalized electrical load.

It is observed in Fig. 10 that relatively large values of $\frac{dP^*}{dR^*_L}$ are obtained prior to $P^* = 1$ implying that thermopower output is sensitive to small changes in load resistance in this region. After attaining a value of 0 near the maximum point, the $\frac{dP^*}{dR^*_L}$ values tend to a constant value. This implies that the thermoelectric power output is less sensitive to changes in electrical loads when they are greater than optimal.

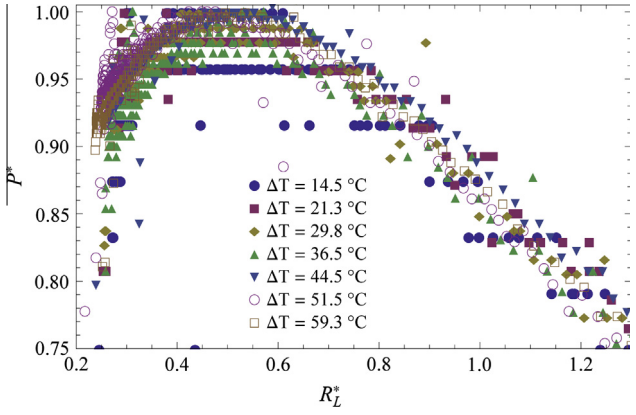

Fig. 8. Normalized load resistance versus normalized thermopower output for thermal input conditions ranging from ΔT = 14.5–59.3 °C.

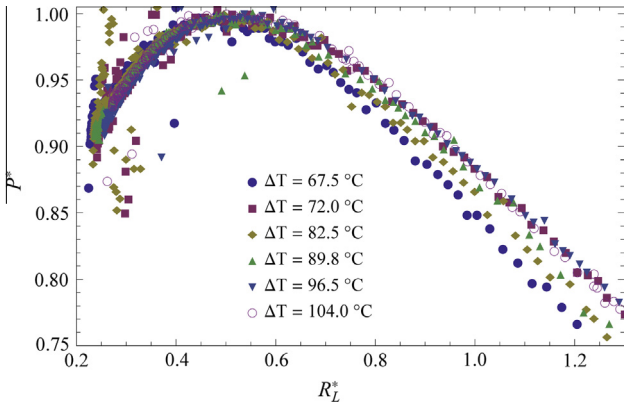

Fig. 9. Normalized load resistance versus normalized thermopower output for thermal input conditions ranging from ΔT = 67.5–104.0 °C.

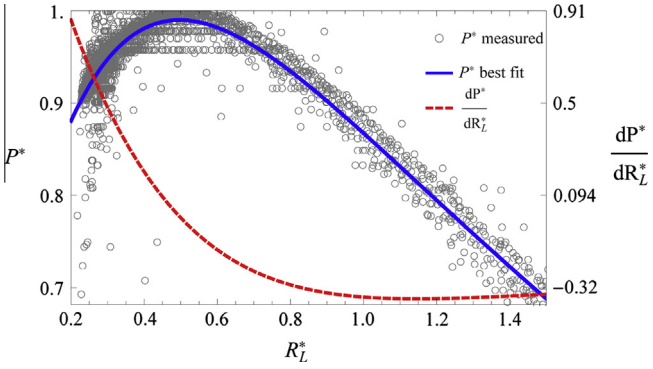

Fig. 10. Best fit normalized thermopower from all thermal conditions tested and its rate of change relative to the electrical load.

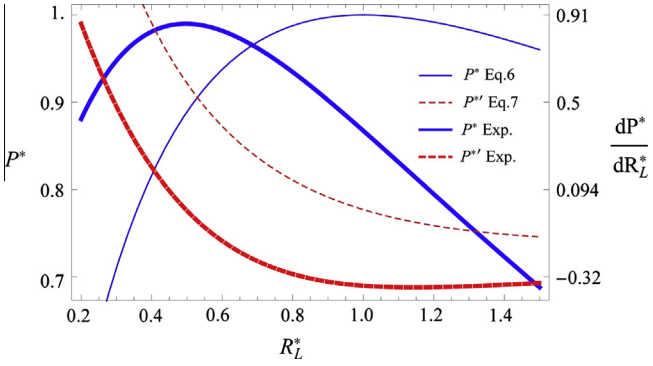

Fig. 11. Theoretical versus experimentally measured normalized power output with respect to normalized electrical load.

In Fig. 11, the best fit curves are compared with those generated by their theoretical values expressed in Eqs. (6) and (7). This comparison shows that the measured normalized optimal electrical load and the theoretical normalized optimal electrical load do not match thereby misaligning the thermopower evolution prediction relative to the electrical load.

It is import to note that the discrepancies between the experimentally measured and predicted P^* curves stem from the theory's optimal load resistance calculation. The differences are attributed to the fact that in the widely used load matching for optimal performance formulation, the thermopower from Eq. (3) is

differentiated with respect to the electrical load in order to identify a local maximum at $R_L = R_i$. In this calculation, the Seebeck coefficient is considered to be constant with respect to the load. This assumption leads to an erroneous result since a material's Seebeck coefficient is observed to decrease with increasing charge carrier concentration Ref. [30] which is variant relative to the load. It is easily shown when differentiating Eq. (3) with the Seebeck coefficient as a variant with respect to the electrical resistance that a negative slope in the Seebeck coefficient relative to load yields an optimal electrical load that is less than the internal resistance. Therefore, the discrepancies in the measured and theorized values of optimal load are attributed to a decrease in Seebeck coefficient due to an increase in charge carrier concentration that is brought upon by an increase in electrical load. An investigation into the modeling of the optimal load with a varying Seebeck coefficient is the subject of a planned future study.

In an effort to modify the theoretical normalized thermopower curve expressed in Eq. (6), the optimal electrical load measured by way of the open circuit voltage is used to scale the thermoelectric power output curve. The normalized optimal electrical load can be calculated with the use of an open circuit voltage measurement such that, from Eq. (8),

$$R^*_{L,opt} = \frac{V^+_{L,opt}}{1 - V^+_{L,opt}}. \tag{10}$$

Eq. (6) is therefore scaled to reach a maximum at the optimal electrical load calculated from Eq. (11). This is accomplished by replacing the variable R^*_L appearing in Eq. (6) with the ratio $R^*_L/R^*_{L,opt}$. In this way, the peak power is aligned with the optimal load as calculated from the open circuit voltage and the entire curve is scaled to this adjustment. The modified normalized power output curve predicting the power to load resistance characteristics near peak power for any temperature input conditions is therefore proposed here as,

$$P^* = \frac{4R^*_L R^*_{L,opt}}{(R^*_{L,opt} + R^*_L)^2}. \tag{11}$$

The rate of change of the modified normalized thermopower with respect to the normalized electrical load is therefore,

$$\frac{dP^*}{dR^*_L} = \frac{4R^*_{L,opt}(R^*_{L,opt} - R^*_L)}{(R^*_{L,opt} + R^*_L)^3}. \tag{12}$$

Since the normalized optimal electrical load is invariant with respect to changing thermal input conditions, the results presented in Eqs. (11) and (12) are deemed valid for any temperature gradient across the module.

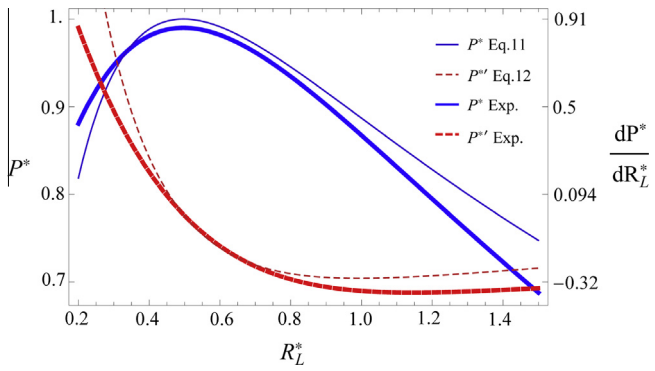

Fig. 12. Modified theoretical power output curve versus the best fit curve from the experimental data obtained from all of the thermal input conditions tested.

The modified theory is compared to the experimentally measured values for all temperature input conditions tested. The results are illustrated in Fig. 12.

The results illustrated in Fig. 12 show that the modified theory of Eq. (11) is in agreement with the measured results near peak power. These results help elucidate the relationship between thermoelectric power and its optimal electrical load thereby providing a stepping stone for a fully analytic theory.

In an effort to further test the developed method of calibration in application and to present a novel thermoelectric conversion of solar energy, a test stand is built which combines solar vacuum tube technology with thermoelectric technology.

5. Solar electric application

The techniques discussed in the previous sections are applied to a solar thermoelectric conversion. To this end, a test stand is built with an artificial light source projected onto a solar vacuum tube in which Acetone vaporization transports heat to a thermoelectric module. The cold side of the module is maintained with forced air convection.

5.1. Experimental setup for solar thermoelectric application

A noncomplicated test stand is built in which the heat source to a thermoelectric module is provided by a solar vacuum tube and the heat rejection on the opposite side of the module is achieved with a CPU heat diffuser. More specifically, a sun lamp ensemble consisting of two 400 W Hydromax high pressure sodium (HPS) bulbs and two 400 W Hydromax metal-halide (MH) bulbs is placed in an upright position facing a Clean Republic solar vacuum tube which is also placed in a vertical position. The sun lamp open facade measures 0.330 m × 0.570 m. The solar tube is a double wall structure with a vacuum between the walls for thermal insulation. The tube is 0.485 m in length with an inner diameter of 43 mm and an outer diameter of 58 mm. A copper sheet measuring 302 mm in length, 21.5 mm in width and 0.06 mm in thickness is rolled and placed inside the tube with a 60 mm × 60 mm × 0.06 mm copper plate soldered to it at the solar tube's opening. A TEG2-07025HT-SS thermoelectric module is placed on top of the tube and in contact with the soldered copper plate. A Cooler Master Hyper 212 CPU Heat pipe is placed on top of the module in order to diffuse heat away from the upper side of the module. Omegatherm 201 thermal compound is placed on the upper and lower surfaces of the module in order to improve thermal transport. The CPU is equipped with a 120 × 120 × 25 mm fan providing 83 cubic feet per minute of ventilation. A 500 g mass is placed on top of the CPU in order to stabilise the apparatus. Inside the enclosed chamber of the tube, 200 ml of Acetone is inserted for its low latent heat of vaporization relative to that of water. The solar tube then effectively acts as a heat pipe at atmospheric pressure circulating thermal energy to the module. A needle size opening is used as a pressure release valve. An aluminum hemispherical reflector of length 0.61 m is placed 35 cm behind the solar tube with the inner concavity facing the tube. The module electrical circuit used, featuring a variable electrical load, is the same as that of Fig. 2. As the lamps are not dimmable, the distance between the tube and the source is varied in an effort to modify and calibrate the light intensity. Two tests are conducted: the first is referred to as "Test 1" in which the sun lamp is a 25 cm horizontal distance from the solar tube; the second test, referred to as "Test 2", has the sun lamp placed 30 cm from the solar tube. The luminosity of the lamp is measured to be 175 ± 10 klx at 25 cm and 120 ± 10 klx at 30 cm. The latter is comparable to direct sunlight, which produces a luminosity known to be between 50 klx and 130 klx [34,35]. However,

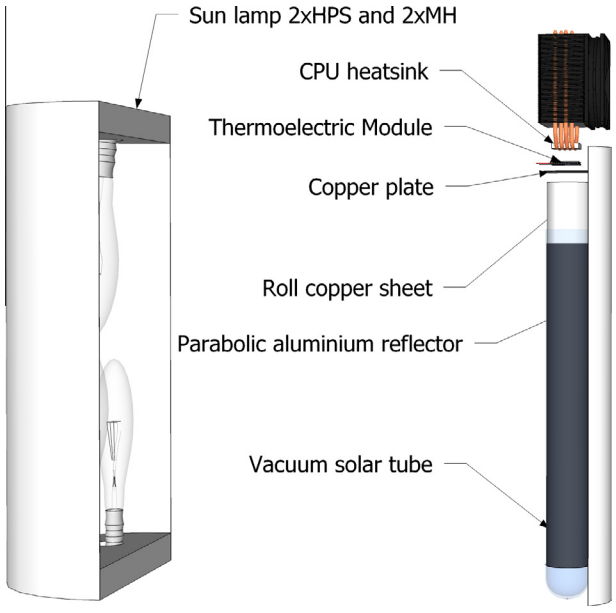

Fig. 13. Schematic representation of the thermoelectric solar electric application.

this comparison is not truly accurate as the light spectrum of the lamp is not the same as the one of the sun. The electrical load resistance for both test cases is increased at a rate of 2.0 ± 1.0 Ω/s. The resultant solar electric setup is illustrated in Fig. 13.

5.2. Results of solar electric application

The results from Test 1 and Test 2 of the solar application each produce thermopower profiles with respect to the electrical load with the same trends as was observed in Section 3.1. That is to say, a sharp increase in thermopower is observed for electrical loads that are less than optimal after which a more gradual decline in thermopower is observed for electrical loads increasing beyond optimal. As illustrated in Fig. 14, there is a significant decrease in peak power in Test 2 due to the increased distance between the sun lamp and the solar tube.

As detailed in Section 1, an important thermopower characteristics for peak power is the optimal electrical load which is measured from the optimal voltage. In this study, these important terms are normalized by the internal resistance and the open circuit voltage respectively. The thermopower characteristics at peak power of test cases Test 1 and Test 2 are provided in Table 2.

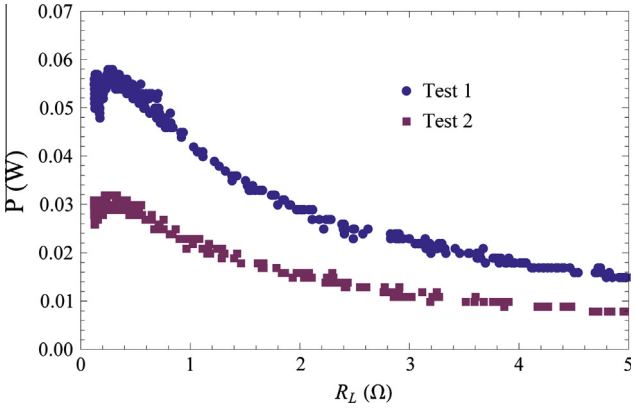

Fig. 14. Effect of an increasing electrical load on thermopower of the solar electric application for two test cases: Test 1 – Sun lamp is 25 cm from the solar tube; Test 2 – Sun lamp is 30 cm from the solar tube.

Table 2
Peak power characteristics of solar thermoelectric application.

	P_{max} (W)	$R_{L,opt}$ (Ω)	$R_{i,opt}$ (Ω)	$R^*_{L,opt}$	V_{oc} (V)	$V_{L,opt}$ (V)	$V^*_{L,opt}$
Test 1	0.058	0.276	0.461	0.599	0.338	0.127	0.376
Test 2	0.032	0.276	0.458	0.602	0.250	0.094	0.376

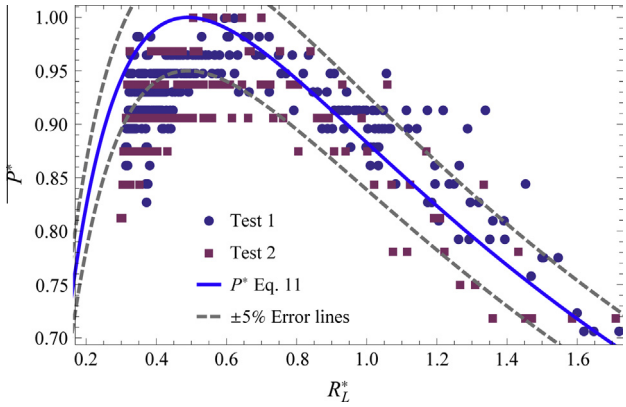

Fig. 15. Normalized thermopower relative to the normalized electrical load of the solar electric application compared with the thermopower curve of Eq. (11).

It is shown in Table 2 that the optimal normalized electrical load is less than unity implying that load matching does not provide peak thermoelectric power. This result is consistent with the results obtained in Section 3. Also in agreement with Section 3 are the normalized power output trends relative to an increasing load. These are presented in Fig. 15 along with the modified power output theory presented by Eq. (11). It is important to recall that in Eq. (11), the normalized optimal electrical load corrects the power output curve presented in Eq. (6) and is solved for using Eq. (10) by way of the optimal load voltage and the open circuit voltage measurements.

The results illustrated in Fig. 15 are indicative of the fact that load matching does not necessarily yield peak thermoelectric power. For the solar electric application of this study, setting the load voltage to half that of the open circuit voltage which corresponds to load matching conditions produces thermopower values that range from approximately 84–92% peak power.

6. Conclusion

The thermopower characteristics of a commercially available thermoelectric module are measured and reported. The first of two test stands in which there is precision control of the injection and the rejection of heat to the module, demonstrates that load matching does not yield peak thermopower for any of the thermal input conditions tested. A simplified normalized power output relation is put forth describing the thermopower output relative to the electrical load near peak power. In this relation, the electrical load is normalized by the internal resistance of the module and the normalized load measured from the optimal load voltage is a required input parameter. It is shown that at peak thermopower, the normalized electrical load and the load voltage to open circuit voltage ratio are each invariant with respect to thermal input conditions. The significance of these results is that, when calibrating a thermoelectric device, it is necessary to identify the optimal electrical load for peak thermopower rather than to assume electric load matching for optimal power output. More importantly, it is

shown that an identified optimal load to internal resistance ratio for a particular thermal input condition can be used to achieve peak thermopower over a large range of thermal input conditions. Furthermore, a solar thermoelectric test apparatus demonstrates that electric load matching can result in power output that is 8% to 16% below peak thermopower.

Acknowledgment

We gratefully thank the Cégep de l'Outaouais and the Fondation du Cégep de l'Outaouais. The authors also thank Stéphane Piché for his technical support.

References

[1] Gou X, Xiao H, Yang S. Modeling, experimental study and optimization on low temperature waste heat thermoelectric generator system. Appl Energy 2010;87:3131–6.
[2] Wee D. Analysis of thermoelectric energy conversion efficiency with linear and nonlinear temperature dependence in material properties. Energy Convers Manage 2012;52:3383–90.
[3] Bélanger S, Gosselin L. Thermoelectric generator sandwiched in a crossflow heat exchanger with optimal connectivity between modules. Energy Convers Manage 2012;52:2911–8.
[4] Hsiao YY, Chang WC, Chen SL. A mathematic model of thermoelectric module with applications on waste heat recovery from automobile engine. Energy 2010;35:1447–54.
[5] Love ND, Szybist JP, Sluder CS. Effect of heat exchanger material and fouling on thermoelectric exhaust heat recovery. Appl Energy 2012;89:322–8.
[6] Karri MA, Thacher EF, Helenbrook BT. Exhaust energy conversion by thermoelectric generator: two case studies. Energy Convers Manage 2011;52:1596–611.
[7] Hsu C-T, Huang G-Y, Chu H-S, Yu B, Yao D-J. Experiments and simulations on low-temperature waste heat harvesting system by thermoelectric power generators. Appl Energy 2011;88:1291–7.
[8] Niu X, Yu J, Wang S. Experimental study on low-temperature waste heat thermoelectric generator. J Power Sources 2009;188:621–6.
[9] O'Shaughnessy SM, Deasy MJ, Kinsella CE, Doyle JV, Robinson AJ. Small scale electricity generation from a portable biomass cookstove: prototype design and preliminary results. Appl Energy 2012. <http://dx.doi.org/10.1016/j.apenergy.2012.07.03>.
[10] Xiao J et al. Thermal design and management for performance optimization of solar thermoelectric generator. Appl Energy 2011. http://dx.doi.org/10.1016/j.apenergy.2011.06.006.
[11] Goldsmid HJ, Giutronich JE, Kaila MM. Solar thermoelectric generation using bismuth telluride alloys. Sol Energy 1980;24:435–40.
[12] Yazawa K, Shakouri A. System optimization of hot water concentrated solar thermoelectric generation. In: Therm Issues Emerg Technol 2010. IEEE ThETA3_056 283.
[13] Yazawa K, Wong VK, Shakouri A. Thermal challenges on solar concentrated thermoelectric CHP systems. In: 13th IEEE ITHERM conference; 2012. 978-1-4244-9532-0/12.
[14] Yu H, Li Y, Shang Y, Su B. Design and investigation of photovoltaic and thermoelectric hybrid power source for wireless sensor networks. In: 3rd IEEE int. conf. on nano/microengineered and molecular systems; 2008. 978-1-4244-1908-1/08.
[15] Daud MMM, Nor NBN, Ibrahim T. Novel hybrid photovoltaic and thermoelectric panel. In: IEEE International power engineering and optimization conference; 2012. 978-1-4673-0662-1/12.
[16] He W, Su Y, Wang YQ, Riffat SB, Ji J. A study on incorporation of thermoelectric modules with evacuated-tube heat-pipe solar collectors. Renew Energy 2012;37:142–9.
[17] Crane DT, Bell LE. Progress towards the performance of a thermoelectric power generator. In: 2006 International conference on thermoelectrics; 2006. 1-4244-0811-3/06.
[18] Kajikawa T, Onishi T. Development for advanced thermoelectric conversion systems. In: 2007 International conference on thermoelectrics; 2008. 978-1-4244-2263-0/08.
[19] Karabetoglu S, Sisman A, Faith Ozturk Z, Sahin T. Characterization of a thermoelectric generator at low temperatures. Energy Convers Manage 2012;62:47–50.
[20] Crane DT, Jackson GS. Optimization of cross flow heat exchangers for thermoelectric waste heat recovery. Energy Convers Manage 2004;45:1565–82.
[21] Rodriguez A, Vian JG, Astrain D, Martinez A. Study of thermoelectric systems applied to electric power generation. Energy Convers Manage 2009;50:1236–43.
[22] Whalena SA, Dykhuizenb RC. Thermoelectric energy harvesting from diurnal heat flow in the upper soil layer. Energy Convers Manage 2012;64:397–402.
[23] Palma P, Pérez-Aparicio JL, Bravo R. Study of hysteretic thermoelectric behavior in photovoltaic materials using the finite method, extended thermodynamics and inverse problems. Energy Convers Manage 2013;65:557–63.
[24] Lesage FJ, Rousse D. Étude expérimentale sur la résistance externe optimale d'un générateur thermoélectrique. In: Récents Progrès en Génie des Procédés; 2011. 101-ISBN 2-910239-75-6, Ed. SFGP, Paris (France).
[25] Lesage FJ, Pagé-Potvin N. Experimental analysis of peak power output of a thermoelectric liquid-to-liquid generator under an increasing electrical load resistance. Energy Convers Manage 2013;66:98–105.
[26] Crane DT, Bell LE. Design to maximize performance of a thermoelectric power generator with a dynamic thermal power source. J Energy Res Technol 2009:131. 012401-1-1-8.
[27] Hsu C-T, Huang G-Y, Chu H-S, Yu B, Yao D-J. An effective Seebeck coefficient obtained by experimental results of a thermoelectric generator module. Appl Energy 2011;88:5173–9.
[28] Dai D, Zhou Y, Liu J. Liquid metal based thermoelectric generation system for waste heat recovery. Renew Energy 2011;36:3530–6.
[29] Hodes M. On one-dimensional analysis of thermoelectric modules [TEMs]. IEEE Trans Compos Pack Technol 2005;28:218–29.
[30] Rowe DM. Thermoelectrics handbook macro to nano. Taylor and Francis Group; 2006.
[31] Eakburanawat J, Boonyaroonate I. Development of a thermoelectric battery charger with microcontroller-based maximum power point tracking technique. Appl Energy 2006;83:687–704.
[32] Hadjistassou C, Kyriakides E, Georgiou J. Designing high efficiency segmented thermoelectric generators. Energy Convers Manage 2013;66:165–72.
[33] Ahiska R, Dislitas S, Omer G. A new method and computer-controlled system for measuring the time constant of real thermoelectric modules. Energy Conv Manage 2012;53:314–21.
[34] Darula S, Kittler R, Gueymard CA. Reference luminous solar constant and solar luminance for illuminance calculations. Sol Energy 2005;79:559–65.
[35] Crawford DL. Photometry: terminology and units in the lighting and astronomical sciences. Observatory 1997;117:14–8.